Circulation Research

ORIGINAL RESEARCH

SARS-CoV-2 Infection Induces Ferroptosis of Sinoatrial Node Pacemaker Cells

Yuling Han,* Jiajun Zhu,* Liuliu Yang,* Benjamin E. Nilsson-Payant,* Romulo Hurtado, Lauretta A. Lacko, Xiaolu Sun, Aravind R. Gade, Christina A. Higgins, Whitney J. Sisso, Xue Dong, Maple Wang, Zhengming Chen, David D. Ho, Geoffrey S. Pitt, Robert E. Schwartz, Benjamin R. tenOever, Todd Evans, Shuibing Chen

BACKGROUND: Increasing evidence suggests that cardiac arrhythmias are frequent clinical features of coronavirus disease 2019 (COVID-19). Sinus node damage may lead to bradycardia. However, it is challenging to explore human sinoatrial node (SAN) pathophysiology due to difficulty in isolating and culturing human SAN cells. Embryonic stem cells (ESCs) can be a source to derive human SAN-like pacemaker cells for disease modeling.

METHODS: We used both a hamster model and human ESC (hESC)–derived SAN-like pacemaker cells to explore the impact of severe acute respiratory syndrome coronavirus 2 (SARS-CoV-2) infection on the pacemaker cells of the heart. In the hamster model, quantitative real-time polymerase chain reaction and immunostaining were used to detect viral RNA and protein, respectively. We then created a dual knock-in *SHOX2:GFP;MYH6:mCherry* hESC reporter line to establish a highly efficient strategy to derive functional human SAN-like pacemaker cells, which was further characterized by single-cell RNA sequencing. Following exposure to SARS-CoV-2, quantitative real-time polymerase chain reaction, immunostaining, and RNA sequencing were used to confirm infection and determine the host response of hESC-SAN–like pacemaker cells. Finally, a high content chemical screen was performed to identify drugs that can inhibit SARS-CoV-2 infection, and block SARS-CoV-2–induced ferroptosis.

RESULTS: Viral RNA and spike protein were detected in SAN cells in the hearts of infected hamsters. We established an efficient strategy to derive from hESCs functional human SAN-like pacemaker cells, which express pacemaker markers and display SAN-like action potentials. Furthermore, SARS-CoV-2 infection causes dysfunction of human SAN-like pacemaker cells and induces ferroptosis. Two drug candidates, deferoxamine and imatinib, were identified from the high content screen, able to block SARS-CoV-2 infection and infection-associated ferroptosis.

CONCLUSIONS: Using a hamster model, we showed that primary pacemaker cells in the heart can be infected by SARS-CoV-2. Infection of hESC-derived functional SAN-like pacemaker cells demonstrates ferroptosis as a potential mechanism for causing cardiac arrhythmias in patients with COVID-19. Finally, we identified candidate drugs that can protect the SAN cells from SARS-CoV-2 infection.

GRAPHIC ABSTRACT: A graphic abstract is available for this article.

Key Words: COVID-19 ■ ferroptosis ■ RNA, viral ■ sinoatrial node ■ stem cells

In This Issue, see p 959 | Meet the First Author, see p 960 | Editorial, see p 978

The sinoatrial node (SAN) represents the primary pacemaker of the heart, situated at the junction of the right atrium and the right common cardinal vein, controlling cardiac rhythm through the downstream components of the cardiac conduction system. It has, however, been challenging to model SAN damage in mammals due to the lack of protocols to isolate and culture SAN cells. Human pluripotent stem cells (hPSCs),

Correspondence to: Shuibing Chen, PhD, Department of Surgery, Weill Cornell Medicine, 1300 York Ave, New York, NY, Email shc2034@med.cornell.edu or Todd Evans, PhD, Department of Surgery, Weill Cornell Medicine, 1300 York Ave, New York, NY, Email tre2003@med.cornell.edu or Benjamin tenOever, PhD, Department of Microbiology, Icahn School of Medicine at Mount Sinai, New York, NY, Email benjamin.tenoever@nyulangone.org or Robert E. Schwartz, PhD, Department of Physiology, Biophysics and Systems Biology, Weill Cornell Medicine, 1300 York Ave, New York, NY, Email res2025@med.cornell.edu
*Y. Han, J. Zhu, L. Yang, B.E. Nilsson-Payant contributed equally.
Supplemental Material is available at https://www.ahajournals.org/doi/suppl/10.1161/CIRCRESAHA.121.320518.
For Sources of Funding and Disclosures, see page 976.

Circulation Research is available at www.ahajournals.org/journal/res

ORIGINAL RESEARCH

Novelty and Significance

What Is Known?

- Increasing evidence suggests that cardiac arrhythmias, including tachycardia and bradycardia, are frequent clinical features of coronavirus disease 2019 (COVID-19).
- Sinus node damage may lead to bradycardia.

What New Information Does This Article Contribute?

- A dual knock-in *SHOX2:GFP; MYH6:mCherry* human embryonic stem cells reporter line was used to purify human sinoatrial node (SAN)–like pacemaker cells.
- The study presents a highly efficient protocol to derive functional human SAN-like pacemaker cells for disease modeling and drug screening.
- Deferoxamine, a ferroptosis inhibitor, blocks severe acute respiratory syndrome coronavirus 2 (SARS-CoV-2) infection, suggesting that SARS-CoV-2 and ferroptosis might have bi-directional interactions.

In this study, using both a hamster model and human embryonic stem cell–SAN–like pacemaker cells, the impact of SARS-CoV-2 infection on the primary pacemaker cells of the heart was explored. Single-cell RNA sequencing validated the expression of SARS-CoV-2 entry factors in SAN-like pacemaker cells, including *ACE2, NRP1, FURIN,* and *CTSL*. Both quantitative real-time polymerase chain reaction and immunostaining confirmed that SARS-CoV-2 readily infects SAN-like pacemaker cells, resulting in marked increase of ferroptosis. Finally, a high content chemical screen identified deferoxamine and imatinib as drugs that block SARS-CoV-2 infection of SAN-like pacemaker cells, as well as SARS-CoV-2 infection-induced ferroptosis.

Nonstandard Abbreviations and Acronyms

COVID-19	coronavirus disease 2019
GPX4	glutathione peroxidase 4
HCN4	hyperpolarization activated cyclic nucleotide gated potassium channel 4
hESCs	human embryonic stem cells
ISL1	insulin gene enhancer protein
MYH6	myosin heavy chain 6
ROS	reactive oxygen species
SAN	sinoatrial node
SARS-CoV-2	severe acute respiratory syndrome coronavirus 2
SARS-N	SARS-CoV-2-nucleocapsid
scRNA-seq	single-cell RNA sequencing
SHOX2:GFP	short stature homeobox 2 green fluorescent protein
TBX3	T-box transcription factor 3

including human embryonic stem cells (hESCs) and induced pluripotent stem cells (hiPSCs), provide a viable strategy to derive functional human SAN-like pacemaker cells. Progress has been made to derive SAN-like pacemaker cells from hESC/hiPSC by directed differentiation,[1] nodal inhibition,[2] and overexpression of *TBX3*[3] or *TBX18*.[4] However, most of these reports either use an *NKX2.5* negative selection approach to enrich nodal-like cells or no selection. To generate a positive selection tool, we created a dual knock-in *SHOX2:GFP; MYH6:mCherry* reporter line using CRISPR/Cas-based gene-targeting techniques that facilitate the quantification and purification of SAN-like pacemaker cells. We used this reporter to develop an efficient strategy to derive functional SAN-like pacemaker cells from hPSCs, which can be applied for disease modeling and drug screening.

Cardiac arrhythmias have been reported in nearly 17% of hospitalized patients with coronavirus disease 2019 (COVID-19), which is associated with a worse disease prognosis. A recent review[5] suggested that supraventricular tachycardia is the most commonly seen electrocardiogram abnormality, which can have many causes including hypoperfusion, electrolyte abnormalities, or anxiety. In addition, sinus bradycardia, a frequent clinical feature of COVID-19, is observed in 56% of hospitalized febrile patients.[6,7] Additional case studies suggest that severe acute respiratory syndrome coronavirus 2 (SARS-CoV-2) infection appears to induce a transient sinus bradycardia in some patients with COVID-19.[8] A retrospective study in Japan showed that relative bradycardia was a common characteristic for 54 patients with polymerase chain reaction (PCR)-confirmed mild-to-moderate COVID-19.[9] Moreover, it was reported that one-third of patients with severe illness developed sinus bradycardia even with no severe myocardial damage or cardiac insufficiency,[6,10] suggesting that there might be an independent cause of sinus bradycardia in patients with COVID-19.

Sinus node damage may lead to bradycardia. No reports exist so far documenting whether the SAN can be infected by SARS-CoV-2 in patients with COVID-19. This can only be determined by biopsy or autopsy and is controversial even for the myocardium. However, postmortem tissues from patients with COVID-19 only evaluate the end-stage of infection, which might not reflect the initial response after acute infection. Therefore, we used a combination of an in vivo hamster model

and hESC-SAN–like pacemaker cells to systematically study the impact of SARS-CoV-2 infection on the SAN. Syrian golden hamsters (*Mesocricetus auratus*) are an established highly susceptible preclinical animal model for SARS-CoV-2 infection.[11–14] Indeed, cardiovascular related complications have been demonstrated in SARS-CoV-2–infected hamsters.[15] We systematically examined the SAN tissue of SARS-CoV-2–infected hamsters and detected viral protein and double-stranded RNA (dsRNA) in HCN4$^+$ (hyperpolarization activated cyclic nucleotide gated potassium channel 4) SAN cells in vivo. Finally, we found that SARS-CoV-2 infection induced ferroptosis of human SAN-like pacemaker cells and identified drugs that can block SARS-CoV-2 infection and ferroptosis.

METHODS

Data and Code Availability

Single-cell RNA sequencing (scRNA-seq) and RNA sequencing (RNA-seq) data are available from the Gene Expression Omnibus (GEO) repository database, accession number GSE193722 (RNA-seq) and GSE193723 (scRNA-seq). The code for scRNA-seq analysis is available at https://github.com/shuibingchen/COVID19-SAN.git.

Animal Studies

Hamsters were housed in cages in the enhanced BSL-3 facility of the Emerging Pathogens Institute at the Icahn School of Medicine at Mount Sinai. All animal experiments were performed according to protocols approved by the Institutional Animal Care and Use Committee and Institutional Biosafety Committee of the Icahn School of Medicine at Mount Sinai (NY). Animals were assigned randomly to the different experimental groups.

The detailed Methods section is available in the Supplemental Materials.

RESULTS

SARS-CoV-2 Is Detected in the Pacemaker of SARS-CoV-2–Infected Hamsters

Due to technical challenges in collecting human SAN autopsy tissues, we used a hamster model, an established highly susceptible preclinical animal model for SARS-CoV-2 infection,[11–14] to examine whether SARS-CoV-2 infects SAN cells in vivo. Male hamsters have been shown to exhibit greater morbidity and susceptibility after SARS-CoV-2 challenge.[16,17] To determine whether pacemaker cells are affected by SARS-CoV-2 infection, male Syrian golden hamsters were intranasally inoculated with SARS-CoV-2 (USA-WA1/2020) and euthanized 48 hours postinfection. The right atrium was isolated from the heart of each animal and quantitative real-time polymerase chain reaction (qRT-PCR) analysis demonstrated the presence of SARS-CoV-2 transcripts in infected animals (Figure 1A). Accordingly, principal component analysis and differential gene expression analysis showed that transcript profiles of right atrium tissue from mock or SARS-CoV-2–infected hamsters clustered separately (Figure 1B). Volcano plots of mock versus SARS-CoV-2–infected hamsters revealed robust induction of transcripts (Figure 1C). As established for SARS-CoV-2 infections in general,[18] chemokines and inflammatory genes were particularly upregulated in infected right atrium tissues (Figure 1D). To gain a clearer understanding of the impact of SARS-CoV-2 specifically on SAN cells, we isolated small regions including the SAN from mock-infected or SARS-CoV-2–infected hamsters (Figure 1E). Immunofluorescence staining confirmed the presence of SARS-CoV-2-Spike protein and viral dsRNA in HCN4$^+$ SAN cells (Figure 1F and 1G and Video S1). Reactive oxygen species (ROS)-related genes were also upregulated in infected right atrium heart tissues (Figure 1H). Together these data suggest that SARS-CoV-2 can in fact infect SAN cells in vivo.

Generation of a Dual Knock-In SHOX2:GFP; MYH6:mCherry hESC Line to Derive Functional Human SAN-Like Pacemaker Cells

To examine if SARS-CoV-2 could infect human SAN cells and explore the virus-host interaction, we sought to develop an efficient protocol to differentiate hESCs to SAN-like pacemaker cells. To quantify and purify SAN-like pacemaker cells, a dual knock-in *SHOX2:GFP; MYH6:mCherry* reporter line was created using CRISPR/Cas9–based gene-targeting techniques (Figure S1A). Through several drug screens (data not shown), we found that an FGFR (fibroblast growth factor receptors) inhibitor, a TGFβ (transforming growth factor-β) inhibitor, and a STAT3 (signal transducer and activator of transcription 3) inhibitor at different concentrations increase the differentiation toward SHOX2-GFP$^+$ cells (Figure S1B, S1C). We tested 5 different combinations of SU5402 (FGFR inhibitor), SB431542 (TGFβ inhibitor) or cucurbitacin (STAT3 inhibitor; Figure S1D through S1F), and developed a stepwise strategy to derive SHOX2:GFP$^+$ (short stature homeobox 2 green fluorescent protein) SAN-like pacemaker cells from hESCs (Figure S1G), including the initial treatment with CHIR-99021, to induce mesoderm differentiation, followed by 2 days treatment with XAV939, SU5402, SB431542, retinoic acid, BMP4 (bone morphogenetic protein 4), and cucurbitacin. Cells were treated for an additional two days with CHIR-99021. Unless otherwise stated, glucose-free RPMI1640 supplemented with lactate was used from day 9 to 11. The cells were maintained in RPMI1640+B27 until analysis at day 20 or day 40. Immunostaining analysis confirmed the

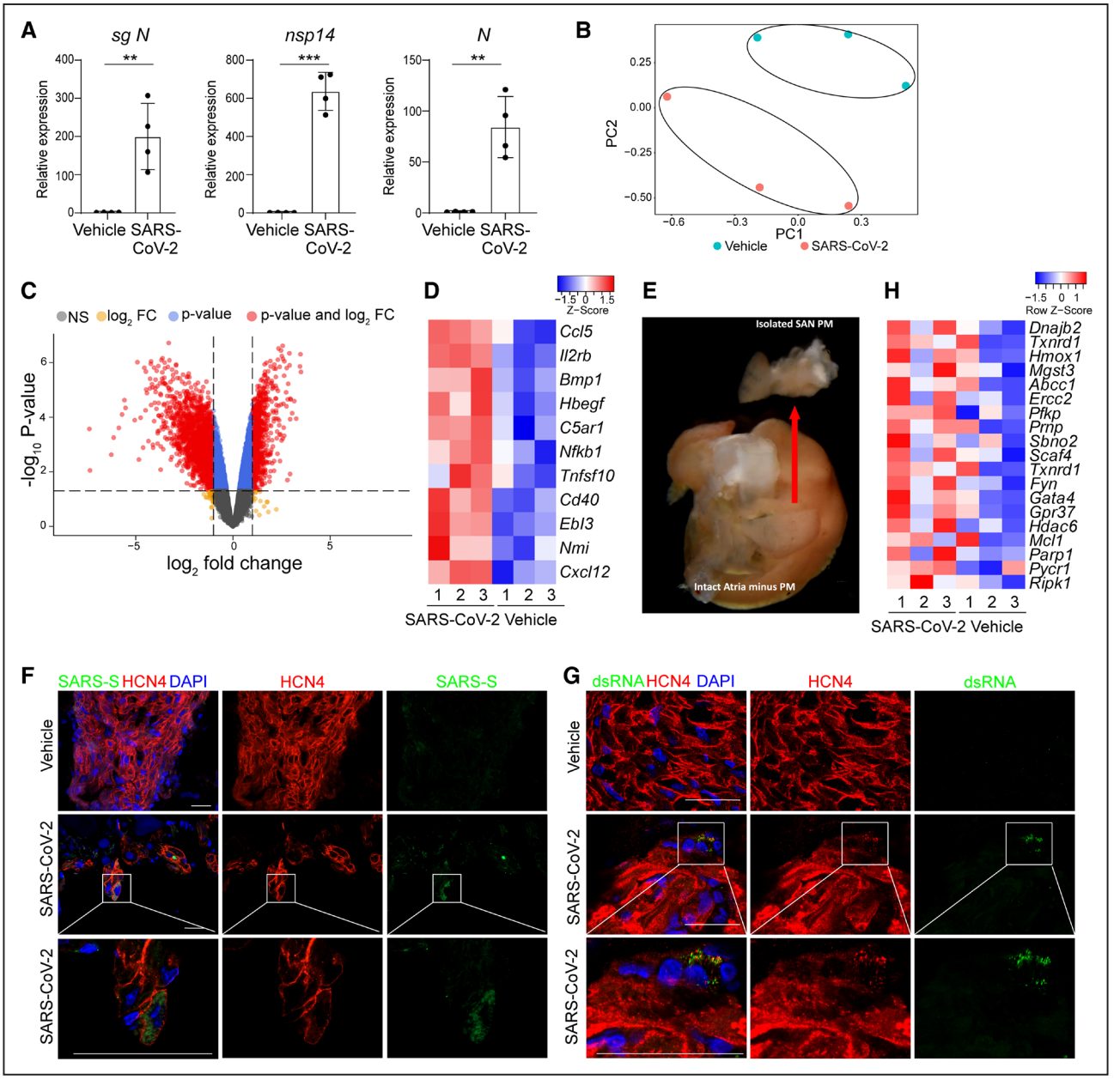

Figure 1. Severe acute respiratory syndrome coronavirus 2 (SARS-CoV-2) is detected in sinoatrial node (SAN) cells of SAN samples from SARS-CoV-2–infected hamsters.

A, Quantitative real-time polymerase chain reaction analysis of SARS-CoV-2 *N* subgenomic RNA (sgRNA), *nsp14,* and *N* transcripts from atria of mock or SARS-CoV-2–infected hamsters. The graph represents the relative RNA expression level normalized to *ACTB.* **B**, Principal component analysis plot of RNA sequencing data from atria of mock or SARS-CoV-2–infected hamsters. **C**, Volcano plot of gene expression in the right atrium of mock or SARS-CoV-2–infected hamsters. **D**, Heatmap of expression levels for cytokines/chemokines and inflammatory genes in the right atrium of mock or SARS-CoV-2–infected hamsters. The high *Z* score indicates high gene expression level. **E**, Representative example of sinoatrial node isolation. **F**, Representative immunostaining of SARS-CoV-2–spike (SARS-S) and HCN4 (hyperpolarization activated cyclic nucleotide gated potassium channel 4) in SAN of mock or SARS-CoV-2–infected hamsters. Lower panels are magnified views of boxed areas highlighted in the middle panels. Scale bars=50 µm. **G**, Representative immunostaining of viral double-stranded RNA (dsRNA) and HCN4 in SAN of mock or SARS-CoV-2–infected hamsters. Lower panels are magnified views of boxed areas highlighted in the middle panels. Scale bars=50 µm. **H**, Heatmap of reactive oxygen species–associated relative gene expression levels in the right atrium of mock or SARS-CoV-2–infected hamsters. The high Z score indicates high gene expression level. N=3 biological samples. DAPI indicates 4′,6-diamidino-2-phenylindole; FC, fold change; n.s, no significance; PC, principal component; and PM, pacemaker. Data are presented as mean±SD. *P* values were calculated by unpaired 2-tailed Student *t* test. ***P*<0.01, ****P*<0.001.

presence of SHOX2:GFP$^+$MYH6 (myosin heavy chain 6):mCherry$^+$ SAN-like pacemaker cells (Figure S2A). MYH6:mCherry$^+$SHOX2:GFP$^-$ cardiomyocytes derived using a standard cardiomyocyte differentiation protocol served as a control (Figure S2B). Flow cytometry analysis further showed that SHOX2:GFP$^+$ cells coexpressed SAN markers, such as HCN1 and ISL1 (insulin gene enhancer protein) (Figure S2C). At day 20 or day 40 of

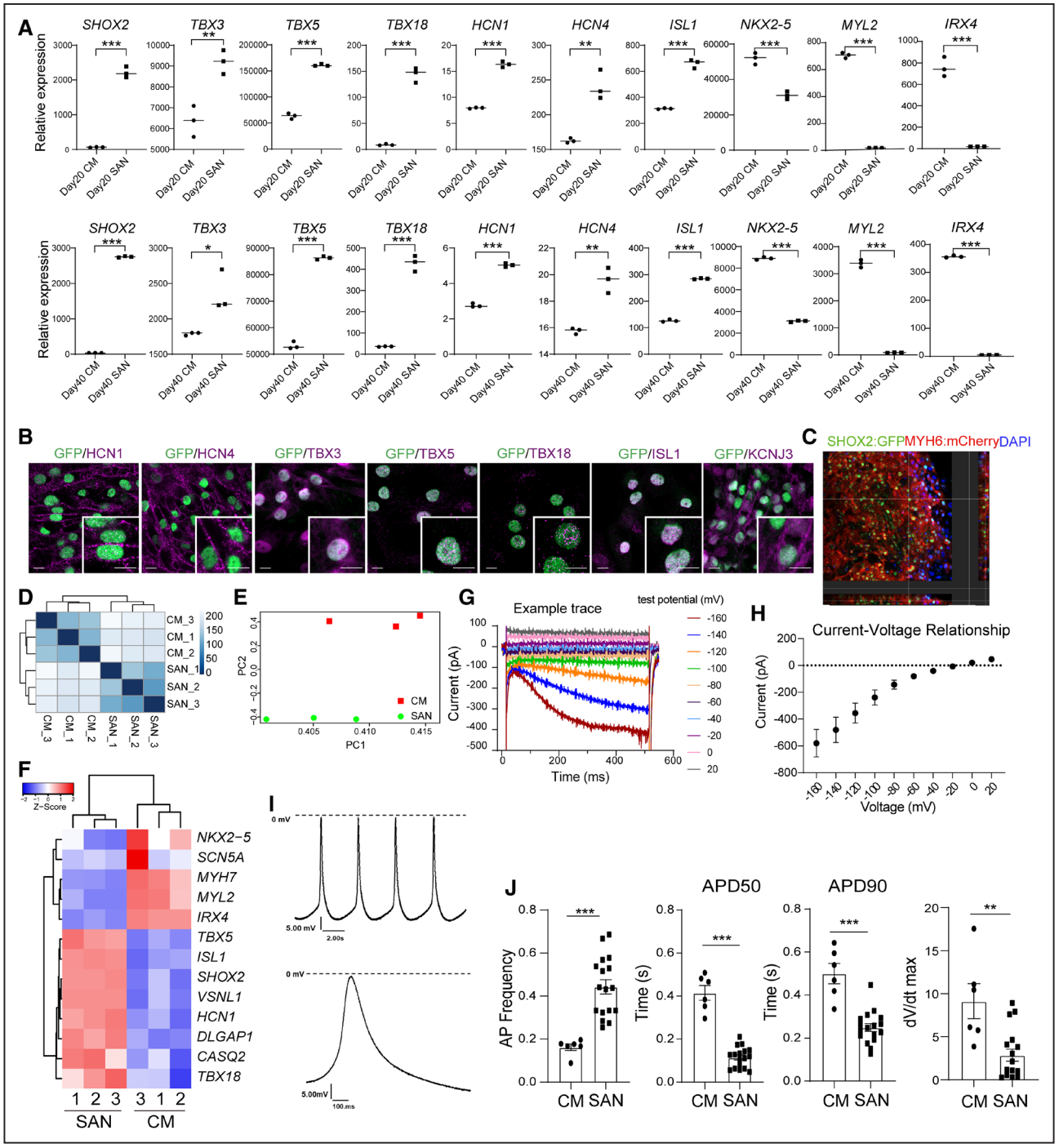

Figure 2. Characterization of human embryonic stem cell (hESC)–sinoatrial node (SAN)-like pacemaker cells.
A, Quantitative real-time polymerase chain reaction analysis comparing day 20 or day 40 SHOX2:GFP$^+$MYH6:mCherry$^+$ (short stature homeobox 2: green fluorescent protein myosin heavy chain 6: mcherry) SAN-like pacemaker cells (SAN) with MYH6:mCherry$^+$SHOX2:GFP$^-$ cardiomyocytes (CMs). Each graph represents the relative RNA expression level normalized to *TBP*. **B**, Representative confocal images of SAN cell markers in hESC-SAN–like pacemaker cells on day 40. Scale bar=10 µm. **C**, Representative confocal images of hESC-SAN–like pacemaker cells. Scale bar=50 µm. **D** and **E**, Clustering analysis (**D**) and principal component analysis plot (**E**) of sorted SHOX2:GFP$^+$MYH6:mCherry$^+$ SAN-like pacemaker cells (SAN) and MYH6:mCherry$^+$SHOX2:GFP$^-$ CMs after RNA sequencing analysis. **F**, Heatmap of SAN and CM cell markers in sorted SHOX2:GFP$^+$MYH6:mCherry$^+$ SAN-like pacemaker cells (SAN) and MYH6:mCherry$^+$SHOX2:GFP$^-$ CMs. The high Z score indicates high gene expression level. **G** and **H**, Electrophysiological recordings of I_f current in hESC-SAN–like pacemaker cells. **I**, Representative recordings of spontaneous action potentials of SHOX2:GFP$^+$MYH6:mCherry$^+$ hESC-SAN–like pacemaker cells. **J**, Quantification of the averaged action potentials recorded from individual hESC-SAN–like pacemaker (n=17) or hESC-CM (n=6) cells and distribution of action potential (AP) frequency, APD50, APD90, dV/dtmax recorded at day 40. N=3 independent experiments. APD indicates action potential duration; DAPI, 4′,6-diamidino-2-phenylindole; HCN, hyperpolarization activated cyclic nucleotide gated potassium channel; ISL1, insulin gene enhancer protein; KCNJ, potassium inwardly rectifying channel subfamily J member; PC, principal component; and TBX, T-box transcription factor. Data are presented as mean±SD. *P* values were calculated by unpaired 2-tailed Student *t* test. **P*<0.05, ***P*<0.01, ****P*<0.001.

differentiation, SHOX2:GFP$^+$MYH6:mCherry$^+$ SAN-like pacemaker cells and MYH6:mCherry$^+$SHOX2:GFP$^-$ cardiomyocytes were analyzed by qRT-PCR. Both day 20 and day 40 SHOX2:GFP$^+$MYH6:mCherry$^+$ SAN-like pacemaker cells show significantly increased expression levels of SAN markers, including *SHOX2*,[19], *TBX3*,[20] *TBX5, TBX18*,[21] *HCN1, HCN4, ISL1*,[22] and decreased expression levels of cardiomyocyte markers, including *NKX2.5*, *MYL2*, and *IRX4* (Figure 2A). Immunostaining validated the coexpression of HCN1, HCN4, TBX3 (T-box transcription factor 3), TBX5, TBX18, ISL1, and KCNJ3 (potassium inwardly rectifying channel subfamily J member 3) in day 20 and day 40 SHOX2:GFP$^+$SAN-like pacemaker cells (Figure 2B and Figure S2D). The derived SAN-like pacemaker cell population adopted 3-dimensional multilayer structures during culture (Figure 2C and Video S2). Transcriptome profiles of SHOX2:GFP$^+$MYH6:mCherry$^+$ SAN-like pacemaker cells and MYH6:mCherry$^+$SHOX2:GFP$^-$ cardiomyocytes sorted at day 20 of differentiation were subsequently compared by RNA-seq (Figure S2E). Principal component analysis and clustering analysis of differentially expressed genes demonstrated clear differences in transcript profiles of MYH6:mCherry$^+$SHOX2:GFP$^+$ and MYH6:mCherry$^+$SHOX2:GFP$^-$ cells, which clustered separately (Figure 2D and 2E). SAN markers, such as *HCN1, TBX5, TBX18*,[23] *ISL1, SHOX2*,[24] *VSNL1, DLGAP1*, and *CASQ2*,[25] were enriched in mCherry$^+$GFP$^+$ SAN-like pacemaker cells, whereas cardiomyocyte markers, including *MYH7, MYL2, IRX4,* and *SCN5A*, were enriched in GFP$^-$mCherry$^+$ cardiomyocytes (Figure 2F). We further monitored the hESC-SAN–like pacemaker cells for the presence of I_f currents by patch-clamp electrophysiology and found the expected inward currents that increased with larger hyperpolarizing steps in 5 of 5 cells tested (example traces and I-V curve of hESC-SAN–like pacemaker in Figure 2G and 2H). In contrast, I_f currents were not observed in hESC-derived ventricular cardiomyocytes (example traces of hESC-cardiomyocyte in Figure S2F). We further monitored the action potentials (APs) to further explore the electrophysiological character of hESC-SAN–like pacemaker cells. Electrophysiological analysis revealed that the SAN-like pacemaker cells had typical pacemaker APs with fast spontaneous APs and short AP durations (Figure 2I). In contrast, the derived ventricular cardiomyocytes displayed relatively fast upstroke velocities and longer AP durations (Figure 2J and Figure S2G). We tested ivabradine, a specific HCN4 channel modulator that has been shown to slow SAN activity on different cell types using a Ca^{2+}-flux assay.[26,27] No significant difference in Ca^{2+}-flux was observed in control and ivabradine-treated hESC-cardiomyocytes. In contrast, a significant reduction of Ca^{2+}-flux was observed in ivabradine-treated hESC-SAN–like pacemaker cells (Figure S2H). Ca^{2+}-flux assays were also applied to monitor the response of hESC-SAN–like pacemaker cells to 1 μmol/L isoproterenol or 5 μmol/L carbachol treatment (Figure S2I). Carbachol treatment had negative chronotropic effects, whereas isoproterenol had positive inotropic effects on hESC-SAN–like pacemaker cells. All experiments, including gene expression profiles, immunostaining, electrophysiological characteristics, and drug sensitivity, together validate the pacemaker identity of our hESC-SAN–like pacemaker cells.

Human SAN-Like Pacemaker Cells Express SARS-CoV-2 Entry Factors

Single-cell RNA-seq was used to further characterize the hESC-derived mCherry$^+$GFP$^+$ population. Five cell clusters were identified, including *SHOX2*$^+$*HCN4*$^+$*TBX5*$^+$ *KCNJ3*$^+$*ISL1*$^+$*MYH6*$^+$ SAN-like pacemaker cells_1 (the major group), SAN-like pacemaker cells_2, *FN1*$^+$*DCN*$^+$ fibroblasts, a small cluster of *FGB*$^+$ smooth muscle cells,[28] and a small unknown population (Figure 3A, S3A and Table S1). The SAN-like pacemaker clusters showed relatively high expression levels of *SHOX2*, *HCN4*, *KCNJ3*, *TBX5*, *ISL1*, and *MYH6* (Figure 3B). Many of the top differentially expressed genes comparing the SAN-like pacemaker groups (Table S1) have known roles in cell cycle or cell division, which likely distinguishes these groups, rather than lineage.

Our hamster studies demonstrated that rodent SAN cells can be infected by SARS-CoV-2 in vivo. To corroborate these finding in a human model system, we first evaluated the scRNA-seq data for the expression of host factors required for viral entry into hESC-SAN–like pacemaker cells. The entry factor NRP1 (neuropilin-1),[29,30] the proteinase CTSL (cathepsin L),[31] and the proprotein convertase FURIN (paired basic amino acid cleaving enzyme)[32] are all expressed by *SHOX2*$^+$ SAN-like pacemaker cells (Figure 3C). Immunostaining validated the expression of ACE2 (angiotensin-converting enzyme 2) and NRP1 in SHOX2:GFP$^+$ SAN-like pacemaker cells (Figure 3D). Previous studies have suggested that scRNA-seq analysis is not sensitive enough to monitor reliably *ACE2* expression.[33] Thus, we confirmed the expression of *ACE2* in MYH6:mCherry$^+$SHOX2:GFP$^+$ SAN-like pacemaker cells by qRT-PCR (Figure S3B).

SARS-CoV-2 Causes Human SAN-Like Pacemaker Cell Dysfunction

To determine the impact of SARS-CoV-2 infection on human SAN-like pacemaker cells, hESC-SAN–like pacemaker cells were infected with SARS-CoV-2 (USA-WA1/2020) at an multiplicity of infection (MOI) of 0.1. qRT-PCR analysis of extracted RNA demonstrated the presence of subgenomic RNA (sgRNA) transcripts, representing the replicating viral RNA at 24 hours postinfection (Figure 4A). Immunostaining assays using SARS-CoV-2-nucleocapsid (SARS-N),

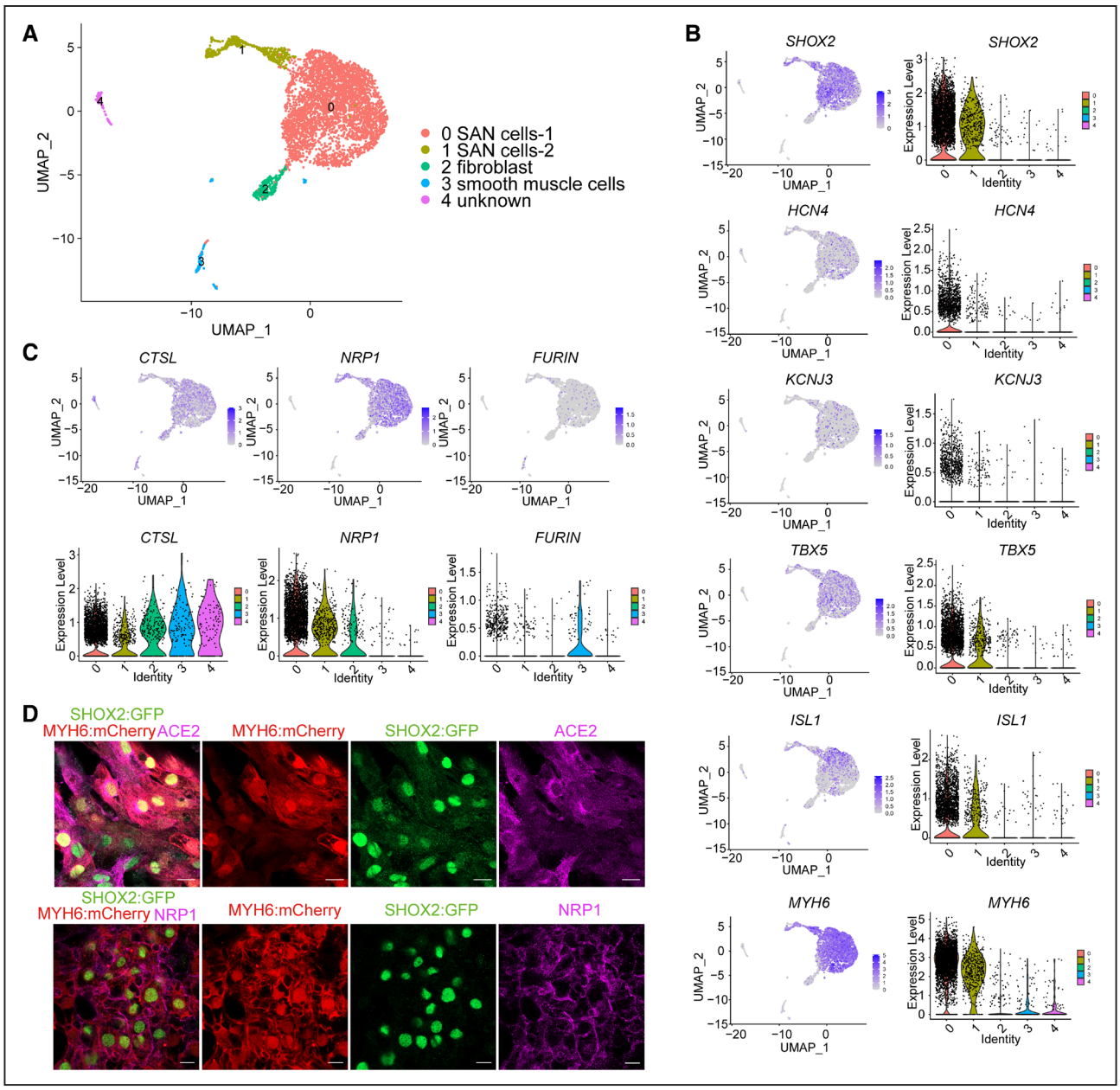

Figure 3. Human sinoatrial node (SAN)–like pacemaker cells express severe acute respiratory syndrome coronavirus 2 (SARS-CoV-2) entry factors.

A, UMAP (uniform manifold approximation and projection) of human embryonic stem cell (hESC)–derived SHOX2:GFP$^+$MYH6:mCherry$^+$ (short stature homeobox 2: green fluorescent protein+ myosin heavy chain 6: mcherry$^+$) SAN-like pacemaker (SAN) cell populations. **B**, UMAP and violin plots of SAN cell markers in hESC-derived SHOX2:GFP$^+$MYH6:mCherry$^+$ SAN-like pacemaker cell populations. **C**, UMAP and violin plots of neuropilin-1 (*NRP1*), *FURIN* and *CTSL* expression levels in hESC-derived SHOX2:GFP$^+$MYH6:mCherry$^+$ SAN-like pacemaker cell populations. **D**, Immunostaining of ACE2 (angiotensin-converting enzyme 2), NRP1 in hESC-SAN–like pacemaker cells. Scale bar=20 μm. N=3 independent experiments.

SARS-CoV-2-Spike (SARS-S), and dsRNA antibodies further confirmed the infection of SARS-CoV-2 in hESC-SAN–like pacemaker cells (Figure 4B). Plaque assays confirmed productive infection of hESC-SAN–like pacemaker cells by demonstrating the presence of infectious progeny virus after SARS-CoV-2 infection (Figure 4C). Electron microscopy showed viral-like particles in hESC-SAN–like pacemaker cells containing myofilaments after infection with SARS-CoV-2 virus (Figure 4D). Functional assays were performed to examine the impact of SARS-CoV-2 on Ca^{2+} influx. SARS-CoV-2 infection fully disrupted the normal cycling Ca^{2+} influx peaks (Figure 4E, Videos S3 and S4). Transcript profiling comparing mock and SARS-CoV-2–infected hESC-SAN–like pacemaker cells aligning transcripts with the viral genome confirmed robust viral replication in hESC-SAN–like pacemaker cells (Figure 4F). Principal component analysis and clustering analysis showed that RNA profiles from mock or SARS-CoV-2–infected hESC-SAN–like pacemaker cells clustered separately

ORIGINAL RESEARCH

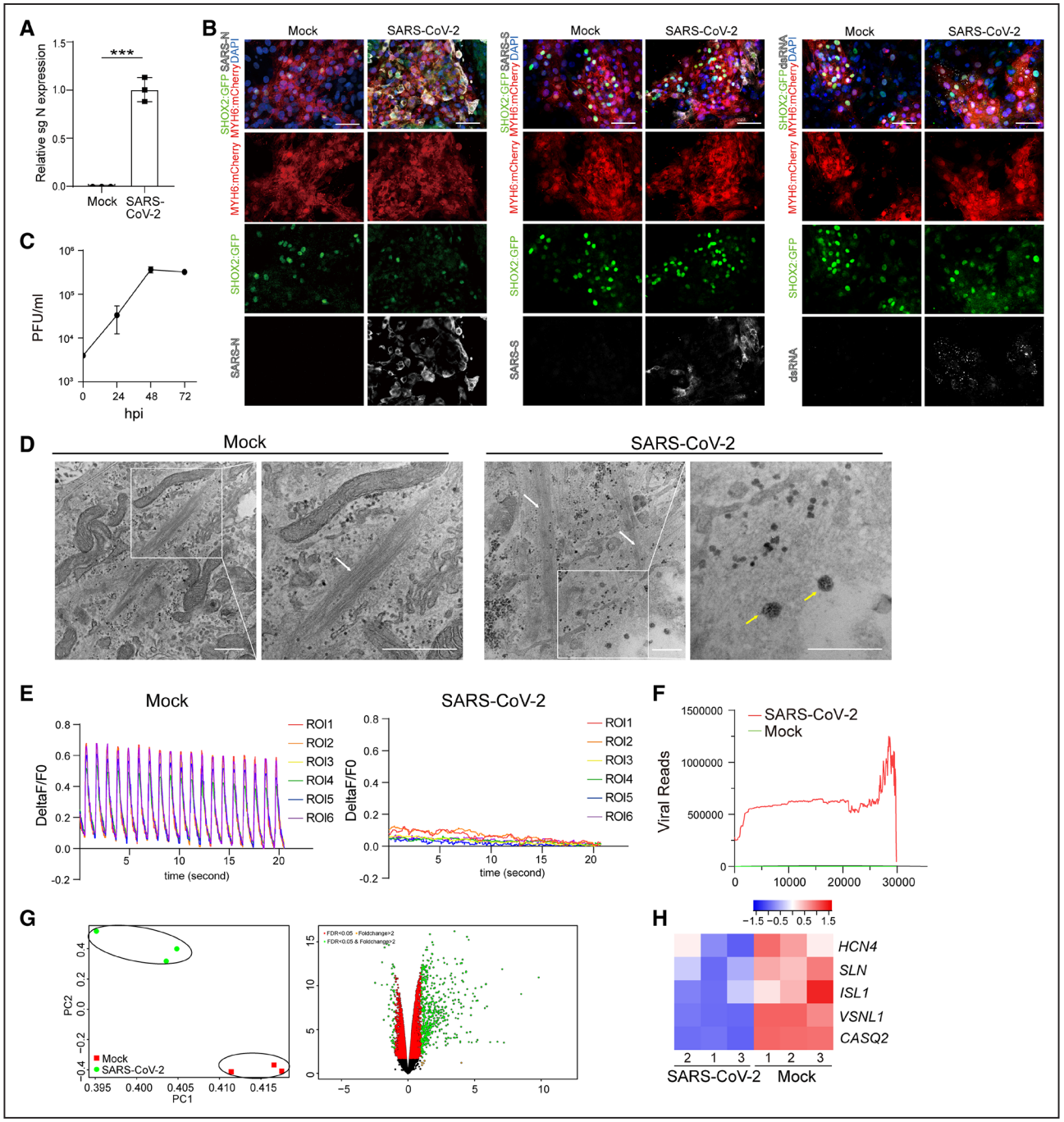

Figure 4. Severe acute respiratory syndrome coronavirus 2 (SARS-CoV-2) infects sinoatrial node (SAN)–like pacemaker cells. **A**, Quantitative real-time polymerase chain reaction analysis of total RNA extracted from human embryonic stem cell (hESC)–SAN–like pacemaker cells at 24 h postinfection (hpi) with SARS-CoV-2 (multiplicity of infection [MOI]=0.1) for viral *N* subgenomic RNA (sgRNA). The graph represents the relative sgRNA level normalized to *ACTB*. **B**, Representative confocal images of hESC-SAN–like pacemaker cells infected with SARS-CoV-2 (MOI=0.1) stained for SARS-CoV-2-Spike (SARS-S), SARS-CoV-2 nucleocapsid (SARS-N), or double-stranded RNA (dsRNA) at 24 hpi. Scale bar=50 µm. **C**, Viral titers of hESC-SAN–like pacemaker cells infected with SARS-CoV-2 for 24, 48, or 72 h (MOI=0.1), quantified by plaque assay. **D**, Representative electron microscopy images of hESC-SAN–like pacemaker cells infected with mock or SARS-CoV-2 (MOI=0.5) at 24 hpi. White arrow: myofilaments. Yellow arrow: SARS-CoV-2. Scale bar=500 nm. **E**, Measurement of calcium influx peaks in mock or SARS-CoV-2 (MOI=0.1) infected hESC-SAN–like pacemaker cells. **F**, Read coverage of the viral genome in SARS-CoV-2–infected hESC-SAN–like pacemaker cells at 24 hpi (MOI=0.1). **G**, Principal component (PC) analysis plot and Volcano plot analysis of RNA sequencing data from mock or SARS-CoV-2 (MOI=0.1) infected hESC-SAN–like pacemaker cells at 24 hpi. **H**, Heatmap of relative SAN marker gene expression levels comparing mock or SARS-CoV-2 (MOI=0.1) infected hESC-SAN–like pacemaker cells at 24 hpi. The high *Z* score indicates high gene expression level. N=3 independent experiments. DAPI indicates 4′,6-diamidino-2-phenylindole; MYH6: mCherry, myosin heavy chain 6: mCherry; PFU, plaque-forming unit; ROI, region of Interest; and SHOX2: GFP, short stature homeobox 2: green fluorescent protein. Data are presented as mean±SD. *P* values were calculated by unpaired 2-tailed Student *t* test. ***$P<0.001$.

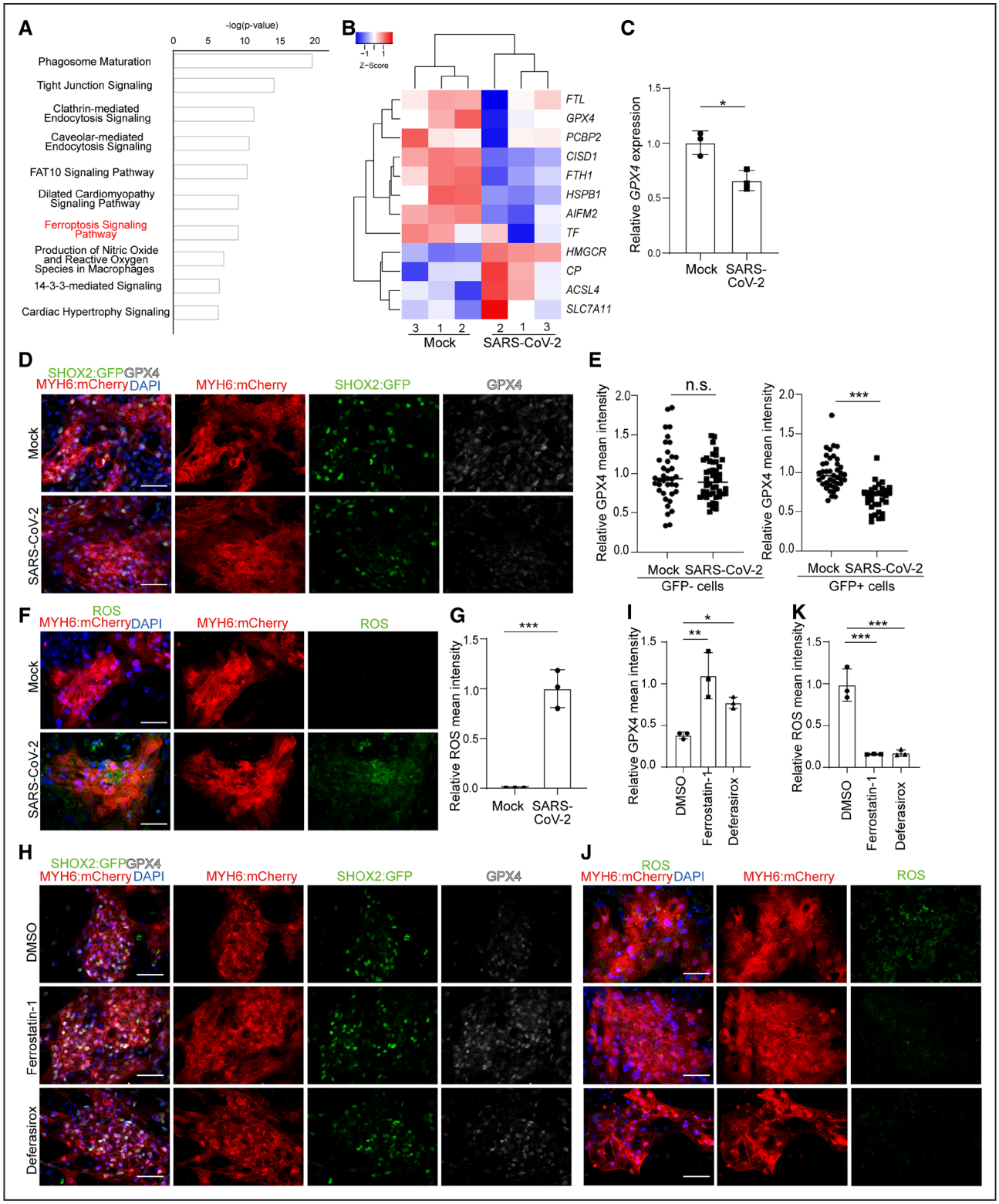

Figure 5. Severe acute respiratory syndrome coronavirus 2 (SARS-CoV-2) infection causes sinoatrial node (SAN)–like pacemaker cell ferroptosis.

A, Ingenuity Pathway Analysis of differential gene expression in mock vs SARS-CoV-2–infected human embryonic stem cell (hESC)–SAN–like pacemaker cells at 24 h postinfection (hpi; multiplicity of infection [MOI]=0.1). **B**, Heatmap comparing expression levels of ferroptosis related genes in mock vs SARS-CoV-2–infected hESC-SAN–like pacemaker cells at 24 hpi (MOI=0.1). The high *Z* score indicates high gene expression level. **C**, Quantitative real-time polymerase chain reaction analysis comparing *GPX4* gene expression levels in mock or SARS-CoV-2–infected hESC-SAN–like pacemaker cells at 24 hpi (MOI=0.1). The graph represents the relative GPX4 (glutathione peroxidase 4) level normalized to *ACTB*. **D** and **E**, Immunostaining (**D**) and quantification (**E**) of GPX4 protein expression levels in mock or SARS-CoV-2–infected SHOX2:GFP$^-$ (short stature homeobox 2: green fluorescent protein) or SHOX2:GFP$^+$ (*Continued*)

(Figure 4G). Some SAN markers, including *HCN4, SLN, ISL1, VSNL1*, and *CASQ2*,[25] were downregulated in the infected hESC-SAN–like pacemaker cells (Figure 4H). Consistent with transcript profiles of infected hESC-cardiomyocytes and heart samples from patients with COVID-19, robust induction of chemokines, including *CCL2*, and inflammatory genes were detected in infected hESC-SAN–like pacemaker cells (Figure S4A and S4B).

SARS-CoV-2 Infection Causes SAN-Like Pacemaker Ferroptosis

Ingenuity Pathway Analysis of differentially expressed genes following SARS-CoV-2 infection of hESC-SAN–like pacemaker cells highlighted pathways involved in the dilated cardiomyopathy signaling pathway and cardiac hypertrophy signaling. Interestingly, the ferroptosis signaling pathway was found to be significantly changed in SARS-CoV-2–infected SAN-like pacemaker cells (Figure 5A). Expression levels for genes involved in ferroptosis, including *SLC7A11*, *ACSL4*, *CP*, *TF*, *PCBP2*, *GPX4*, and *HSBP1* are significantly changed (Figure 5B). qRT-PCR and immunostaining assays (Figure 5C through 5E) further validated decreased levels of *GPX4* transcripts or protein, respectively, a key factor regulating ferroptosis,[34–36] in SARS-CoV-2–infected SAN-like pacemaker cells. The decreased expression level of GPX4 (glutathione peroxidase 4) was only found in infected GFP^+ cells but not in infected GFP^- cells (Figure 5E). Moreover, SARS-CoV-2–infected SAN-like pacemaker cells showed accumulation of ROS, one of the hallmarks of ferroptosis (Figure 5F and 5G). Two known ferroptosis inhibitors, ferrostatin-1 and deferasirox, each rescued expression levels of GPX4 (Figure 5H and 5I) and blocked the ROS induced by SARS-CoV-2 infection (Figure 5J and 5K). The expression of cleaved CASP3 (caspase 3), a classic apoptotic marker, was not significantly changed in SARS-CoV-2–infected SAN-like pacemaker cells (Figure S4C and S4D), which contrasts with the response to infection of hESC-cardiomyocytes.[37] In addition, the expression level of GPX4 in SARS-CoV-2–infected hESC-cardiomyocytes was not significantly changed (Figure S4E and S4F). Furthermore, we examined the expression levels of *GPX4* in hESC-derived lung alveolar organoids, pancreatic endocrine cells, liver organoids, and dopamine neurons upon SARS-CoV-2 infection, as well as in lung tissues from COVID-19 or non–COVID-19 subjects. *GPX4* expression was not significantly changed between uninfected and SARS-CoV-2–infected conditions in any of these organoids or tissues, indicating that SARS-CoV-2 infection–causing ferroptosis is relatively specific for hESC-SAN–like pacemaker cells (Figure S4G). The SAN differentiation protocol involves a metabolic-based selection step, which has been suggested to produce a heart failure-like phenotype.[38] To confirm that SARS-CoV-2 infection and ferroptosis are independent of metabolic-based selection, we also infected the hESC-SAN–like pacemaker population without metabolic-based selection (Figure S1G). Consistent with the experiments using hESC-SAN–like pacemaker cells derived with metabolic selection protocol, SARS-N viral antigen was detected in $SHOX2{:}GFP^+MYH6{:}mCherry^+$ SAN-like pacemaker cells derived without metabolic selection (Figure S4H). Decreased GPX4 expression was also seen in SARS-CoV-2–infected hESC-SAN–like pacemaker cells derived without metabolic selection (Figure S4I and S4J). Thus, SARS-CoV-2 infection and infection-induced ferroptosis in hESC-SAN–like pacemaker cells are independent of metabolic-based selection.

Chemical Screen Identifies Drug Candidates Blocking SARS-CoV-2 Infection in SAN Cells

To identify drug candidates capable of protecting SAN cells from SARS-CoV-2 infection, hESC-SAN–like pacemaker cells were treated with 10 μM of a library of Food and Drug Administration–approved drugs. Four hours posttreatment, SAN-like pacemaker cells were infected with SARS-CoV-2 at MOI=0.1. At 24 hours postinfection, SAN-like pacemaker cells were stained with SARS-N antibody. The percentage of $SARS\text{-}N^+$ cells was used for quantification. The wells in which a Z score<—2 were chosen as primary hit drugs (Figure 6A). The hits were evaluated for potency and cytotoxicity at different concentrations. Two drugs were confirmed to decrease the percentage of $SARS\text{-}N^+$ cells through a dose-dependent manner, independent of cytotoxicity, including deferoxamine (EC_{50}=4.56 μM, Figure 6B and 6C) and imatinib (EC_{50}=0.61 μM, 50% cytotoxic concentration [CC_{50}]=32.60 μM, Figure 6D and 6E). The percentage of $SARS\text{-}N^+$ cells in wells treated with 50 μM deferoxamine, or 10 μM imatinib

Figure 5 Continued. hESC-SAN–like pacemaker cells at 24 hpi (MOI=0.1). Scale bar=50 μm. Each dot in the graph represents the relative GPX4 level for individual $SHOX2{:}GFP^+$ or $SHOX2{:}GFP^-$ cells. **F** and **G**, Immunostaining (**F**) and quantification (**G**) of reactive oxygen species (ROS) in mock and SARS-CoV-2–infected hESC-SAN–like pacemaker cells at 24 hpi (MOI=0.1). Scale bar=50 μm. **H** and **I**, Immunostaining (**H**) and quantification (**I**) of GPX4 protein expression level in dimethyl sulfoxide (DMSO), 10 μM ferrostatin-1 or 50 μM deferasirox-treated hESC-SAN–like pacemaker cells at 24 hpi with SARS-CoV-2 (MOI=0.1). Scale bar=50 μm. **J** and **K**, Immunostaining (**J**) and quantification (**K**) of ROS in DMSO, 10 μM ferrostatin-1 or 50 μM deferasirox-treated hESC-SAN–like pacemaker cells at 24 hpi with SARS-CoV-2 (MOI=0.1). Scale bar=50 μm. N=3 independent experiments. Data are presented as mean±SD. DAPI indicates 4′,6-diamidino-2-phenylindole; FAT10, human leukocyte antigen (HLA)-F adjacent transcript 10; and MYH6: mCherry, myosin heavy chain 6: mcherry. For comparison of 2 groups, *P* values were calculated by unpaired 2-tailed Student *t* test. For comparison of 3 groups, *P* values were calculated by 1-way ANOVA with an indicated control. n.s indicates no significance, $^*P<0.05$, $^{**}P<0.01$, $^{***}P<0.001$.

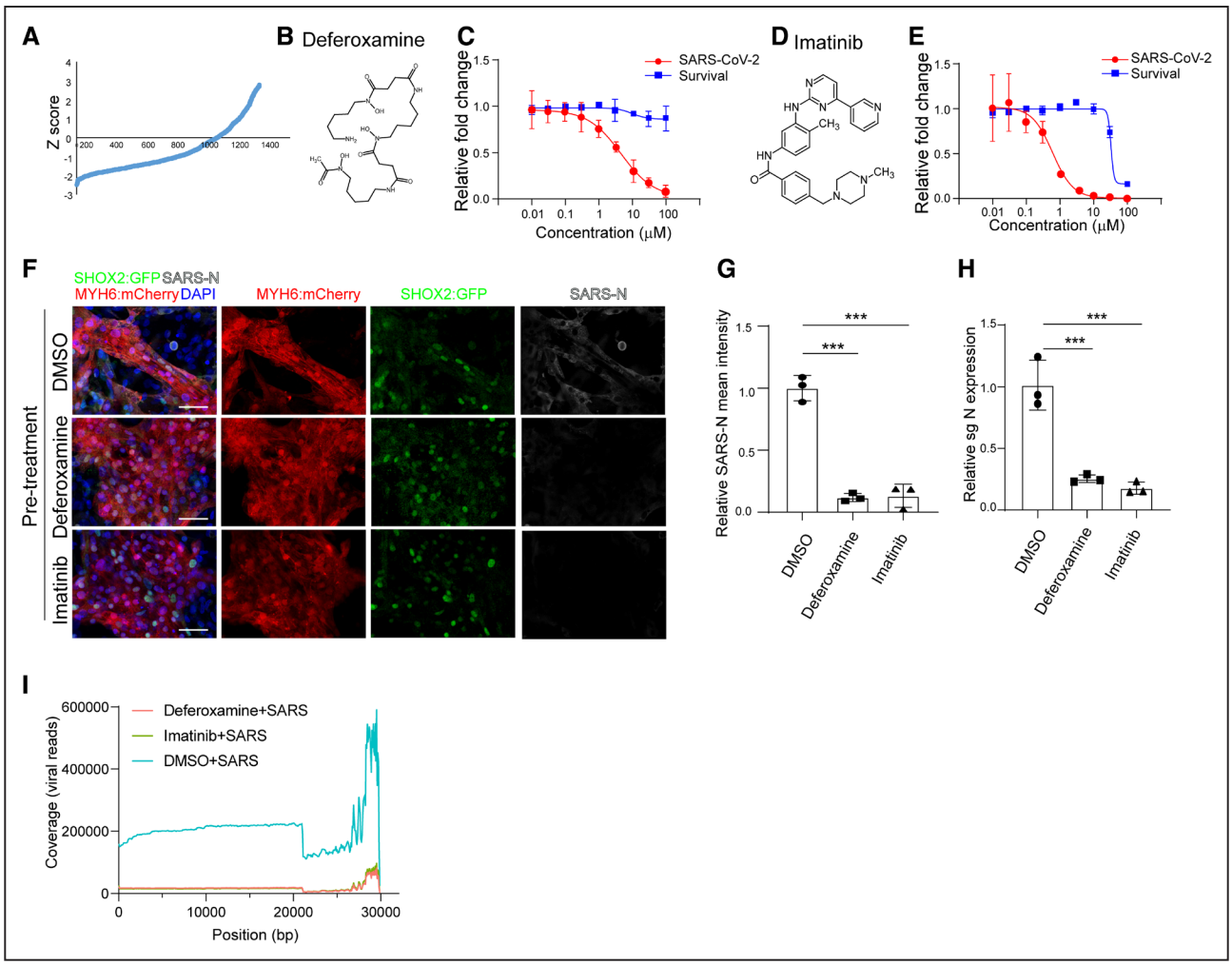

Figure 6. A high content chemical screen to identify anti–severe acute respiratory syndrome coronavirus 2 (SARS-CoV-2) drugs using human embryonic stem cell (hESC)–sinoatrial node (SAN)–like pacemaker cells.
A, The primary screening result. *x* axis represents the compound number. *y* axis represents the *Z* score. **B**, Chemical structure of deferoxamine. **C**, Efficacy and cytotoxicity curves for deferoxamine. **D**, Chemical structure of imatinib. **E**, Efficacy and cytotoxicity curves for imatinib. **F** and **G**, Immunostaining (**F**) and the quantification (**G**) of dimethyl sulfoxide (DMSO), 50 μM deferoxamine-treated, or 10 μM imatinib-treated hESC-SAN–like pacemaker cells at 24 hours postinfection (hpi) with SARS-CoV-2 (multiplicity of infection [MOI]=0.1). Scale bar=50 μm. **H**, Quantitative real-time polymerase chain reaction analysis of total RNA extracted from DMSO, 50 μM deferoxamine-treated, or 10 μM imatinib-treated hESC-SAN–like pacemaker cells at 24 hpi with SARS-CoV-2 (MOI=0.1) for viral *N* subgenomic RNA (sgRNA). The graph represents the mean sgRNA level normalized to *ACTB*. **I**, Read coverage of the viral genome from DMSO, 50 μM deferoxamine-treated, or 10 μM imatinib-treated hESC-SAN–like pacemaker cells at 24 hpi with SARS-CoV-2 (MOI=0.1). N=3 independent experiments. Data were presented as mean±SD. DAPI, indicates 4′,6-diamidino-2-phenylindole; MYH6: mCherry, myosin heavy chain 6: mcherry; SARS-N, SARS-CoV-2 nucleocapsid; sgN, sub genomic SARS-CoV-2 nucleocapsid RNA; and SHOX2:GFP, short stature homeobox 2: green fluorescent protein. *P* values were calculated by 1-way ANOVA with an indicated control. ***$P<0.001$.

before infection (pretreatment condition) was significantly lower than the percentage of SARS-N$^+$ cells in wells treated with dimethyl sulfoxide (DMSO; Figure 6F and 6G). qRT-PCR assays further validated the decrease of N subgenomic RNA transcripts for cells treated with either of the 2 drugs before infection (Figure 6H). We also added deferoxamine and imatinib 4 hours after infection (postinfection condition). At 24 hours after infection, we found that imatinib, but not deferoxamine, significantly decreased the percentage of SARS-N$^+$ cells and subgenomic RNA (Figure S5A through S5C). Consistently, both deferoxamine and imatinib decreased virus infection in hESC-cardiomyocytes when applied preinfection, while only imatinib decreased virus infection in hESC-cardiomyocytes when applied postinfection (Figure S5D through S5I). RNA-seq was applied to analyze transcript profiles for the DMSO, deferoxamine, or imatinib-treated SAN-like pacemaker cells. The alignment to SARS-CoV-2 viral genome further validated the significant decrease of SARS-CoV-2–associated transcripts in deferoxamine or imatinib treated SAN-like pacemaker cells (Figure 6I).

ORIGINAL RESEARCH

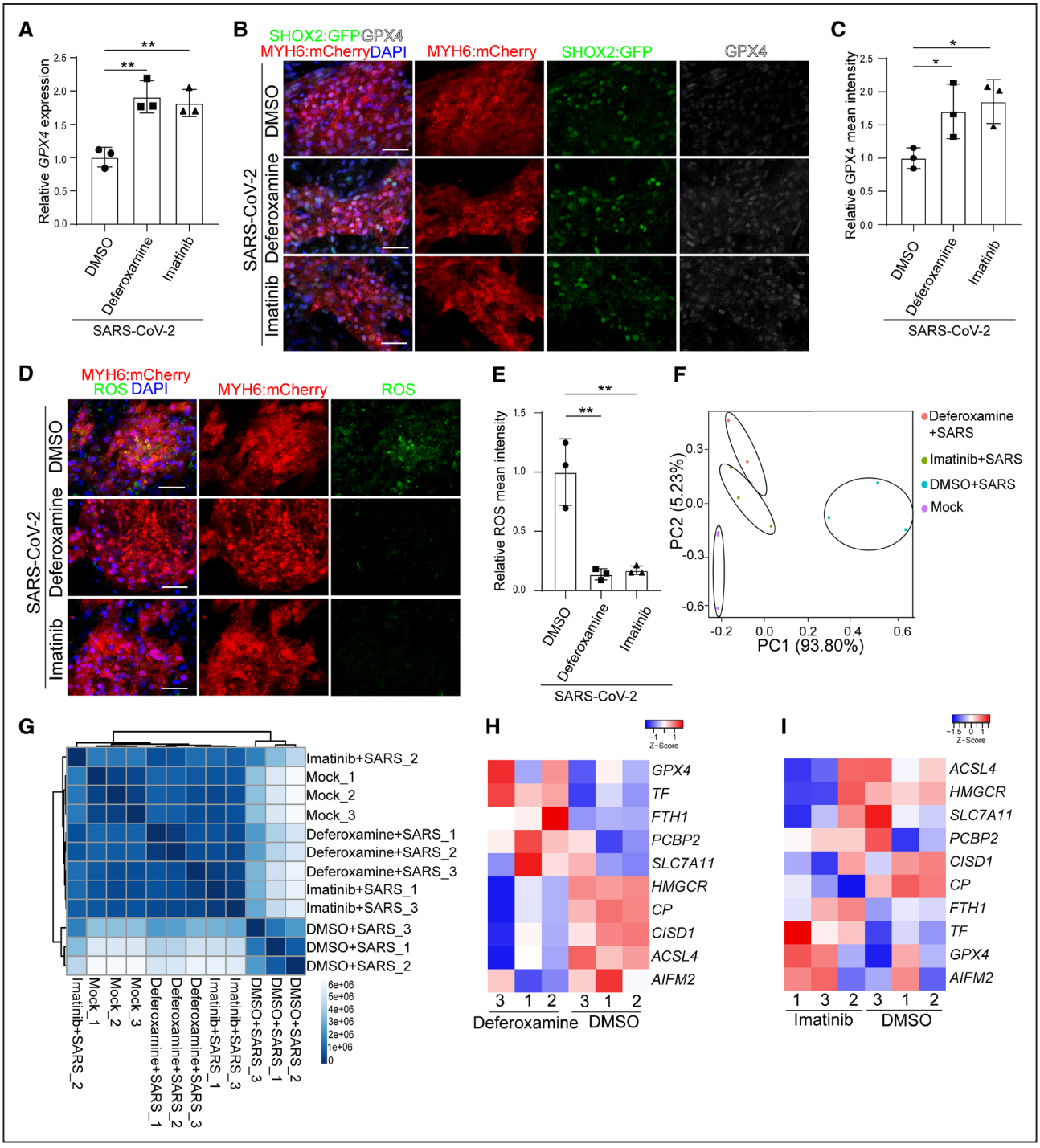

Figure 7. Deferoxamine and imatinib inhibit severe acute respiratory syndrome coronavirus 2 (SARS-CoV-2) infection–induced ferroptosis.

A, Quantitative real-time polymerase chain reaction analysis of *GPX4* expression levels in dimethyl sulfoxide (DMSO), 50 μM deferoxamine-treated, or 10 μM imatinib-treated human embryonic stem cell (hESC)–sinoatrial node (SAN)–like pacemaker cells at 24 hours postinfection (hpi) with SARS-CoV-2 (multiplicity of infection [MOI]=0.1). The graph represents the RNA level normalized to *ACTB*. **B** and **C**, Immunostaining (**B**) and quantification (**C**) of GPX4 expression levels in DMSO, 50 μM deferoxamine-treated, or 10 μM imatinib-treated hESC-SAN–like pacemaker cells at 24 hpi with SARS-CoV-2 (MOI=0.1). Scale bar=50 μm. **D** and **E**, Immunostaining (**D**) and quantification (**E**) of reactive oxygen species (ROS) in DMSO, 50 μM deferoxamine-treated, or 10 μM imatinib-treated hESC-SAN–like pacemaker cells at 24 hpi with SARS-CoV-2 (MOI=0.1). Scale bar=50 μm. **F** and **G**, Principal component (PC) analysis plot (**F**) and cluster analysis (**G**) of gene expression profiles of mock and DMSO, 50 μM deferoxamine-treated, or 10 μM imatinib-treated hESC-SAN–like pacemaker cells at 24 hpi with SARS-CoV-2 (MOI=0.1). **H** and **I**, Heatmap of ferroptosis-associated gene expression levels in DMSO, 50 μM deferoxamine-treated, or 10 μM imatinib-treated hESC-SAN–like pacemaker cells at 24 hpi with SARS-CoV-2 (MOI=0.1). The high *Z* score indicates high gene expression level. N=3 independent experiments. Data are presented as mean±SD. DAPI indicates 4′,6-diamidino-2-phenylindole; GPX, glutathione peroxidase; MYH6: mCherry, myosin heavy chain 6: mcherry; and SHOX2:GFP, short stature homeobox 2: green fluorescent protein. *P* values were calculated by 1-way ANOVA with an indicated control. **P*<0.05 and ***P*<0.01.

Deferoxamine and Imatinib Block SARS-CoV-2 Infection–Associated Ferroptosis

Deferoxamine and imatinib were evaluated for their capacities to block SARS-CoV-2 infection-mediated ferroptosis. qRT-PCR assays showed higher expression levels of *GPX4* with either 50 μM deferoxamine or 10 μM imatinib treatment (Figure 7A) following SARS-CoV-2 infection. Immunostaining further confirmed the higher expression levels of GPX4 (Figure 7B and 7C) and lower levels of ROS (Figure 7D through 7E) in 50 μM deferoxamine+SARS-CoV-2 or 10 μM imatinib+SARS-CoV-2 treated SAN-like pacemaker cells. Principal component analysis and clustering analysis of RNA-seq profiles showed that deferoxamine or imatinib treated SAN-like pacemaker cells clustered very close to mock-treated SAN-like pacemaker cells compared with SARS-CoV-2+DMSO–treated cells (Figure 7F and 7G and Figure S6A). RNA-seq profiles validated the decreased levels of ferroptosis-associated genes in SARS-CoV-2–infected SAN-like pacemaker cells treated with 50 μM deferoxamine (Figure 7H) or 10 μM imatinib (Figure 7I) compared with DMSO treated SAN-like pacemaker cells, respectively. Together, the data show that deferoxamine and imatinib block SARS-CoV-2 infection and subsequent ferroptosis. Consistently, SARS-CoV-2–infected SAN-like pacemaker cells treated with either 50 μM deferoxamine (Figure S6B and S6C) or 10 μM imatinib (Figure S6D and S6E) showed significantly decreased expression levels of chemokines and inflammatory genes compared to DMSO-treated infected SAN-like pacemaker cells.

DISCUSSION

Comprising the functional pacemaker of the heart, SAN cells play a critical role in controlling heartbeat rhythm. However, insight into molecular and cellular features of human SAN biology has been challenging due to technical difficulty in isolating and culturing SAN cells. hPSCs, which have unlimited proliferation capacity and the ability to differentiate to any cell lineage, provide a valuable resource to generate human SAN-like pacemaker cells. Some progress has been made by either directed differentiation[1,2] or overexpression of SAN-associated transcriptional factors.[3,4] However, the field has previously lacked a positive selection strategy to obtain highly enriched SAN-like pacemaker cells for disease modeling.[1,21] For this purpose, we created a dual knock-in *SHOX2:GFP; MYH6:mCherry* reporter line and developed an efficient protocol to derive and purify human SAN-like pacemaker cells. The derived GFP$^+$ cells are enriched for expression of SHOX2, TBX3, TBX5, TBX18, HCN1, HCN4, ISL1, and depleted for cardiomyocyte muscle markers MYL2 and IRX4 (iroquois homeobox 4). Furthermore, electrophysiological experiments and action potentials further validated the SAN cell identity of the GFP$^+$ cells. To perform single-cell electrophysiology, the cells were dissociated into single cells and recorded at room temperature. We note that the beat-to-beat interval of nodal-like cells under these conditions is longer than seen under physiological conditions.

Recent studies have reported that patients with COVID-19 with severe illness developed a variety of arrhythmias including sinus bradycardia independent of the clinical characteristics of myocarditis or myocardial infarction,[10] suggesting possible defects of the cardiac conduction system in patients with COVID-19. There could be many causes for SAN abnormalities, including a variety of secondary effects, most notably inflammation from the cytokine storm. However, it is also possible that defects might be caused by direct viral infection in patients with COVID-19. Due to challenges in collecting SAN tissues of patients with COVID-19, we analyzed SARS-CoV-2–infected hamsters, a broadly used model to study SARS-CoV-2 pathogenesis and antiviral drug testing. qRT-PCR detected viral transcripts in the right atrium of hamster hearts and immunostaining further demonstrated the presence of SARS-CoV-2 spike protein and dsRNA in HCN4$^+$ SAN cells. The current study focused on male hamsters, which are reported to show greater morbidity and susceptibility after SARS-CoV-2 infection.[16,17] Additional work is needed to examine the SAN of SARS-CoV-2–infected female hamsters. Therefore, it is a reasonable possibility that patients with COVID-19 could suffer arrhythmia from direct SAN infection.

We, therefore, explored the impact of SARS-CoV-2 infection on hPSC-SAN–like pacemaker cells and found that SARS-CoV-2 infection causes ferroptosis. Although SARS-CoV-2 has been reported to induce cellular apoptosis,[39] this is to our knowledge the first report of SARS-CoV-2–mediated ferroptosis. Ferroptosis is mainly caused by the accumulation of lipid ROS in cells, resulting in fatal lipid peroxidation.[40] Iron, the overload of which causes ferroptosis, has been reported to be an important mechanism contributing to the pathogenesis of various viruses, including hepatitis B virus,[41] hepatitis C virus,[42] human immunodeficiency virus (HIV-1),[43] and human cytomegalovirus.[44] Ferroptosis of SAN-like pacemaker cells induced by SARS-CoV-2 infection might contribute to the pathogenesis of patients with COVID-19 and explain some of the cardiac arrhythmias observed in patients. Interestingly, although many types of cells/organoids, including hESC-SAN–like pacemaker cells, cardiomyocytes,[45] hPSC-derived lung alveolar organoids,[46] hPSC-derived pancreatic endocrine cells,[47] hPSC-derived liver organoids,[47] can be infected by SARS-CoV-2, ferroptosis is only detected in SARS-CoV-2–infected hESC-SAN–like pacemaker cells, indicating a cell type–specific response to SARS-CoV-2 infection.

We further adapted the hESC-SAN–like pacemaker cell platform to perform a high throughput screen for

drugs inhibiting SARS-CoV-2 infections. One hit compound, imatinib, was identified in our previous studies using a lung or colon organoid-based viral entry screen,[46] highlighting the anti-viral activity of imatinib across multiple tissues and organs. Another hit compound, deferoxamine, is a medication that binds iron, is used to treat iron overdose,[48] and is a known inhibitor of ferroptosis. Suggesting one possible mechanism, treatment with deferoxamine decreases the RNA and protein level of CTSL, a key factor involved in SARS-CoV-2 entry (Figure S7A through S7D). Moreover, deferoxamine treatment significantly decreases SARS-CoV-2 entry in both hESC-SAN–like pacemaker cells and hESC-cardiomyocytes using our previously reported platform[46] (Figure S7E and S7F).

ARTICLE INFORMATION

Received November 17, 2021; revision received February 17, 2022; accepted February 24, 2022.

Affiliations

Department of Surgery (Y.H., J.Z., L.Y., R.H., L.A.L., W.J.S., X.D., T.E., S.C.), Cardiovascular Research Institute (X.S., A.R.G., G.S.P.), Department of Population Health Sciences (Z.C.), Division of Gastroenterology and Hepatology, Department of Medicine (R.E.S.), and Department of Physiology, Biophysics and Systems Biology (R.E.S.), Weill Cornell Medicine, New York, NY. Department of Microbiology, Icahn School of Medicine at Mount Sinai, New York, NY (B.E.N.-P., B.R.T.). Department of Microbiology, New York University (B.E.N.-P., C.A.H., B.R.T.). Aaron Diamond AIDS Research Center, Columbia University Vagelos College of Physicians and Surgeons, New York, NY (M.W., D.D.H.).

Author Contributions

S. Chen, T. Evans, B.R. tenOever, R.E. Schwartz, and D.D. Ho conceived and designed the experiments. J. Zhu performed sinoatrial node (SAN)–like pacemaker cells and cardiomyocyte differentiation. Y. Han, L. Yang, and M. Wang performed staining, quantitative real-time polymerase chain reaction (qRT-PCR), chemical screening, and RNA sequencing (RNA-seq) analysis. C.A. Higgins, B.E. Nilsson-Payant performed severe acute respiratory syndrome coronavirus 2 (SARS-CoV-2) infection experiments. R. Hurtado dissected SAN tissues from hamsters. L.A. Lacko, W.J. Sisso, and X. Dong performed confocal imaging. X. Sun, A.R. Gade, and G.S. Pitt performed electrophysiology experiments. J. Zhu performed the bioinformatics analyses. Z. Chen performed the biostatistical analysis.

Sources of Funding

This work was supported by the American Heart Association (18CSA34080171, S. Chen, T. Evans), Department of Surgery, Weill Cornell Medicine (T. Evans, S. Chen), Tri-Institutional Stem Cell Institute (2021-026, S. Chen), National Institute of Diabetes and Digestive and Kidney Diseases (NIDDK) (R01DK130454, R01DK119667-02S1, S. Chen), National Heart, Lung, and Blood Institute (NHLBI) (R01HL151190, R01HL160089, G.S. Pitt), Bill & Melinda Gates Foundation (INV-018723, S. Chen, T. Evans, R.E. Schwartz) and (National Cancer Institute [NCI] R01CA234614, National Institute of Allergy and Infectious Diseases [NIAID] 2R01AI107301 and NIDDK R01DK121072 and 1RO3DK117252), Department of Medicine, Weill Cornell Medicine (R.E. Schwartz), by the Defense Advanced Research Projects Agency (DARPA) (DARPA-16-35-INTERCEPT-FP-006, B.R.T.). S. Chen and R.E. Schwartz are supported as Irma Hirschl Trust Research Award Scholars. Y. Han is an NYSTEM Stem Cell Biology Scholar (DOH01-TRAIN3-2016-00004). L.A. Lacko is supported by Eunice Kennedy Shriver National Institute of Child Health and Human Development (NICHD) (1F32HD096810-01) and the Weill Cornell Medicine Research Assistance for Primary Parents Award. T. Evans is supported by an Outstanding Investigator Award (R35 HL135778).

Disclosures

R.E. Schwartz is on the scientific advisory board of Miromatrix Inc and a consultant and speaker for Alnylam Pharmaceuticals. T. Evans and S. Chen are founding owners of OncoBeat, LLC. A patent has been filled for Compositions and methods for generation of sinoatrial node-like cells and their use in drug discovery. The other authors report no conflicts.

Supplemental Materials

Expanded Materials and Methods
Figures S1–S8
Tables S1–S4
Videos S1–S4
References 14,18,45,49–51

REFERENCES

1. Protze SI, Liu J, Nussinovitch U, Ohana L, Backx PH, Gepstein L, Keller GM. Sinoatrial node cardiomyocytes derived from human pluripotent cells function as a biological pacemaker. *Nat Biotechnol.* 2017;35:56–68. doi: 10.1038/nbt.3745
2. Yechikov S, Kao HKJ, Chang CW, Pretto D, Zhang XD, Sun YH, Smithers R, Sirish P, Nolta JA, Chan JW, et al. NODAL inhibition promotes differentiation of pacemaker-like cardiomyocytes from human induced pluripotent stem cells. *Stem Cell Res.* 2020;49:102043. doi: 10.1016/j.scr.2020.102043
3. Zhao H, Wang F, Zhang W, Yang M, Tang Y, Wang X, Zhao Q, Huang C. Overexpression of TBX3 in human induced pluripotent stem cells (hiPSCs) increases their differentiation into cardiac pacemaker-like cells. *Biomed Pharmacother.* 2020;130:110612. doi: 10.1016/j.biopha.2020.110612
4. Gorabi AM, Hajighasemi S, Tafti HA, Atashi A, Soleimani M, Aghdami N, Saeid AK, Khori V, Panahi Y, Sahebkar A. TBX18 transcription factor overexpression in human-induced pluripotent stem cells increases their differentiation into pacemaker-like cells. *J Cell Physiol.* 2019;234:1534–1546. doi: 10.1002/jcp.27018
5. Long B, Brady WJ, Bridwell RE, Ramzy M, Montrief T, Singh M, Gottlieb M. Electrocardiographic manifestations of COVID-19. *Am J Emerg Med.* 2021;41:96–103. doi: 10.1016/j.ajem.2020.12.060
6. Coromilas EJ, Kochav S, Goldenthal I, Biviano A, Garan H, Goldbarg S, Kim JH, Yeo I, Tracy C, Ayanian S, et al. Worldwide survey of COVID-19-associated arrhythmias. *Circ Arrhythm Electrophysiol.* 2021;14:e009458. doi: 10.1161/CIRCEP.120.009458
7. Capoferri G, Osthoff M, Egli A, Stoeckle M, Bassetti S. Relative bradycardia in patients with COVID-19. *Clin Microbiol Infect.* 2021;27:295–296. doi: 10.1016/j.cmi.2020.08.013
8. Amaratunga EA, Corwin DS, Moran L, Snyder R. Bradycardia in patients with COVID-19: a calm before the storm? *Cureus.* 2020;12:e8599. doi: 10.7759/cureus.8599
9. Ikeuchi K, Saito M, Yamamoto S, Nagai H, Adachi E. Relative bradycardia in patients with mild-to-moderate coronavirus disease, Japan. *Emerg Infect Dis.* 2020;26:2504–2506. doi: 10.3201/eid2610.202648
10. Hu L, Gong L, Jiang Z, Wang Q, Zou Y, Zhu L. Clinical analysis of sinus bradycardia in patients with severe COVID-19 pneumonia. *Crit Care.* 2020;24:257. doi: 10.1186/s13054-020-02933-3
11. Sia SF, Yan LM, Chin AWH, Fung K, Choy KT, Wong AYL, Kaewpreedee P, Perera RAPM, Poon LLM, Nicholls JM, et al. Pathogenesis and transmission of SARS-CoV-2 in golden hamsters. *Nature.* 2020;583:834–838. doi: 10.1038/s41586-020-2342-5
12. Imai M, Iwatsuki-Horimoto K, Hatta M, Loeber S, Halfmann PJ, Nakajima N, Watanabe T, Ujie M, Takahashi K, Ito M, et al. Syrian hamsters as a small animal model for SARS-CoV-2 infection and countermeasure development. *Proc Natl Acad Sci USA.* 2020;117:16587–16595. doi: 10.1073/pnas.2009799117
13. Rosenke K, Meade-White K, Letko M, Clancy C, Hansen F, Liu Y, Okumura A, Tang-Huau TL, Li R, Saturday G, et al. Defining the Syrian hamster as a highly susceptible preclinical model for SARS-CoV-2 infection. *Emerg Microbes Infect.* 2020;9:2673–2684. doi: 10.1080/22221751.2020.1858177
14. Hoagland DA, Møller R, Uhl SA, Oishi K, Frere J, Golynker I, Horiuchi S, Panis M, Blanco-Melo D, Sachs D, et al. Leveraging the antiviral type I interferon system as a first line of defense against SARS-CoV-2 pathogenicity. *Immunity.* 2021;54:557–570.e555. doi: 10.1016/j.immuni.2021.01.017
15. Rizvi ZA, Dalal R, Sadhu S, Kumar Y, Srivastava T, Gupta SK, Agarwal S, Tripathy MR, Yadav AK, Medigeshi GR, et al. Immunological and cardiovascular pathologies associated with SARS-CoV-2 infection in golden syrian hamster. *bioRxiv.* 2021:2021.2001.2011.426080. doi: 10.1101/2021.01.11.426080

16. Yuan L, Zhu H, Zhou M, Ma J, Chen R, Chen Y, Chen L, Wu K, Cai M, Hong J, et al. Gender associates with both susceptibility to infection and pathogenesis of SARS-CoV-2 in Syrian hamster. *Signal Transduct Target Ther*. 2021;6:136. doi: 10.1038/s41392-021-00552-0
17. Dhakal S, Ruiz-Bedoya CA, Zhou R, Creisher PS, Villano JS, Littlefield K, Ruelas Castillo J, Marinho P, Jedlicka AE, Ordonez AA, et al; Johns Hopkins COVID-19 Hamster Study Group. Sex differences in lung imaging and SARS-CoV-2 antibody responses in a COVID-19 golden syrian hamster model. *mBio*. 2021;12:e0097421. doi: 10.1128/mBio.00974-21
18. Blanco-Melo D, Nilsson-Payant BE, Liu WC, Uhl S, Hoagland D, Møller R, Jordan TX, Oishi K, Panis M, Sachs D, et al. Imbalanced host response to SARS-CoV-2 drives development of COVID-19. *Cell*. 2020;181:1036–1045.e9. doi: 10.1016/j.cell.2020.04.026
19. Sun C, Yu D, Ye W, Liu C, Gu S, Sinsheimer NR, Song Z, Li X, Chen C, Song Y, et al. The short stature homeobox 2 (Shox2)-bone morphogenetic protein (BMP) pathway regulates dorsal mesenchymal protrusion development and its temporary function as a pacemaker during cardiogenesis. *J Biol Chem*. 2015;290:2007–2023. doi: 10.1074/jbc.M114.619007
20. Jung JJ, Husse B, Rimmbach C, Krebs S, Stieber J, Steinhoff G, Dendorfer A, Franz WM, David R. Programming and isolation of highly pure physiologically and pharmacologically functional sinus-nodal bodies from pluripotent stem cells. *Stem Cell Reports*. 2014;2:592–605. doi: 10.1016/j.stemcr.2014.03.006
21. Kapoor N, Liang W, Marbán E, Cho HC. Direct conversion of quiescent cardiomyocytes to pacemaker cells by expression of Tbx18. *Nat Biotechnol*. 2013;31:54–62. doi: 10.1038/nbt.2465
22. Hoffmann S, Berger IM, Glaser A, Bacon C, Li L, Gretz N, Steinbeisser H, Rottbauer W, Just S, Rappold G. Islet1 is a direct transcriptional target of the homeodomain transcription factor Shox2 and rescues the Shox2-mediated bradycardia. *Basic Res Cardiol*. 2013;108:339. doi: 10.1007/s00395-013-0339-z
23. Goodyer WR, Beyersdorf BM, Paik DT, Tian L, Li G, Buikema JW, Chirikian O, Choi S, Venkatraman S, Adams EL, et al. Transcriptomic profiling of the developing cardiac conduction system at single-cell resolution. *Circ Res*. 2019;125:379–397. doi: 10.1161/CIRCRESAHA.118.314578
24. Chandler NJ, Greener ID, Tellez JO, Inada S, Musa H, Molenaar P, Difrancesco D, Baruscotti M, Longhi R, Anderson RH, et al. Molecular architecture of the human sinus node: insights into the function of the cardiac pacemaker. *Circulation*. 2009;119:1562–1575. doi: 10.1161/CIRCULATIONAHA.108.804369
25. Liang D, Xue J, Geng L, Zhou L, Lv B, Zeng Q, Xiong K, Zhou H, Xie D, Zhang F, et al. Cellular and molecular landscape of mammalian sinoatrial node revealed by single-cell RNA sequencing. *Nat Commun*. 2021;12:287. doi: 10.1038/s41467-020-20448-x
26. Yaniv Y, Sirenko S, Ziman BD, Spurgeon HA, Maltsev VA, Lakatta EG. New evidence for coupled clock regulation of the normal automaticity of sinoatrial nodal pacemaker cells: bradycardic effects of ivabradine are linked to suppression of intracellular Ca^{2+} cycling. *J Mol Cell Cardiol*. 2013;62:80–89. doi: 10.1016/j.yjmcc.2013.04.026
27. DiFrancesco D. The role of the funny current in pacemaker activity. *Circ Res*. 2010;106:434–446. doi: 10.1161/CIRCRESAHA.109.208041
28. Sahara M, Santoro F, Sohlmér J, Zhou C, Witman N, Leung CY, Mononen M, Bylund K, Gruber P, Chien KR. Population and single-cell analysis of human cardiogenesis reveals unique LGR5 ventricular progenitors in embryonic outflow tract. *Dev Cell*. 2019;48:475–490.e7. doi: 10.1016/j.devcel.2019.01.005
29. Cantuti-Castelvetri L, Ojha R, Pedro LD, Djannatian M, Franz J, Kuivanen S, van der Meer F, Kallio K, Kaya T, Anastasina M, et al. Neuropilin-1 facilitates SARS-CoV-2 cell entry and infectivity. *Science*. 2020;370:856–860. doi: 10.1126/science.abd2985
30. Daly JL, Simonetti B, Klein K, Chen KE, Williamson MK, Antón-Plágaro C, Shoemark DK, Simón-Gracia L, Bauer M, Hollandi R, et al. Neuropilin-1 is a host factor for SARS-CoV-2 infection. *Science*. 2020;370:861–865. doi: 10.1126/science.abd3072
31. Ou X, Liu Y, Lei X, Li P, Mi D, Ren L, Guo L, Guo R, Chen T, Hu J, et al. Characterization of spike glycoprotein of SARS-CoV-2 on virus entry and its immune cross-reactivity with SARS-CoV. *Nat Commun*. 2020;11:1620. doi: 10.1038/s41467-020-15562-9
32. Shang J, Wan Y, Luo C, Ye G, Geng Q, Auerbach A, Li F. Cell entry mechanisms of SARS-CoV-2. *Proc Natl Acad Sci USA*. 2020;117:11727–11734. doi: 10.1073/pnas.2003138117
33. Hou YJ, Okuda K, Edwards CE, Martinez DR, Asakura T, Dinnon KH 3rd, Kato T, Lee RE, Yount BL, Mascenik TM, et al. SARS-CoV-2 reverse genetics reveals a variable infection gradient in the respiratory tract. *Cell*. 2020;182:429–446.e14. doi: 10.1016/j.cell.2020.05.042
34. Yang WS, SriRamaratnam R, Welsch ME, Shimada K, Skouta R, Viswanathan VS, Cheah JH, Clemons PA, Shamji AF, Clish CB, et al. Regulation of ferroptotic cancer cell death by GPX4. *Cell*. 2014;156:317–331. doi: 10.1016/j.cell.2013.12.010
35. Friedmann Angeli JP, Schneider M, Proneth B, Tyurina YY, Tyurin VA, Hammond VJ, Herbach N, Aichler M, Walch A, Eggenhofer E, et al. Inactivation of the ferroptosis regulator Gpx4 triggers acute renal failure in mice. *Nat Cell Biol*. 2014;16:1180–1191. doi: 10.1038/ncb3064
36. Ingold I, Berndt C, Schmitt S, Doll S, Poschmann G, Buday K, Roveri A, Peng X, Porto Freitas F, Seibt T, et al. Selenium utilization by GPX4 is required to prevent hydroperoxide-induced ferroptosis. *Cell*. 2018;172:409–422.e21. doi: 10.1016/j.cell.2017.11.048
37. Stockwell BR, Friedmann Angeli JP, Bayir H, Bush AI, Conrad M, Dixon SJ, Fulda S, Gascón S, Hatzios SK, Kagan VE, et al. Ferroptosis: a regulated cell death nexus linking metabolism, redox biology, and disease. *Cell*. 2017;171:273–285. doi: 10.1016/j.cell.2017.09.021
38. Davis J, Chouman A, Creech J, Monteiro da Rocha A, Ponce-Balbuena D, Jimenez Vazquez EN, Nichols R, Lozhkin A, Madamanchi NR, Campbell KF, et al. In vitro model of ischemic heart failure using human induced pluripotent stem cell-derived cardiomyocytes. *JCI Insight*. 2021;6:134368. doi: 10.1172/jci.insight.134368
39. Ren Y, Shu T, Wu D, Mu J, Wang C, Huang M, Han Y, Zhang XY, Zhou W, Qiu Y, et al. The ORF3a protein of SARS-CoV-2 induces apoptosis in cells. *Cell Mol Immunol*. 2020;17:881–883. doi: 10.1038/s41423-020-0485-9
40. Hadian K, Stockwell BR. SnapShot: ferroptosis. *Cell*. 2020;181:1188–1188.e1. doi: 10.1016/j.cell.2020.04.039
41. Gao YH, Wang JY, Liu PY, Sun J, Wang XM, Wu RH, He XT, Tu ZK, Wang CG, Xu HQ, et al. Iron metabolism disorders in patients with hepatitis B-related liver diseases. *World J Clin Cases*. 2018;6:600–610. doi: 10.12998/wjcc.v6.i13.600
42. Fujita N, Sugimoto R, Urawa N, Araki J, Mifuji R, Yamamoto M, Horiike S, Tanaka H, Iwasa M, Kobayashi Y, et al. Hepatic iron accumulation is associated with disease progression and resistance to interferon/ribavirin combination therapy in chronic hepatitis C. *J Gastroenterol Hepatol*. 2007;22:1886–1893. doi: 10.1111/j.1440-1746.2006.04759.x
43. Traoré HN, Meyer D. The effect of iron overload on in vitro HIV-1 infection. *J Clin Virol*. 2004;31(Suppl 1):S92–S98. doi: 10.1016/j.jcv.2004.09.011
44. Crowe WE, Maglova LM, Ponka P, Russell JM. Human cytomegalovirus-induced host cell enlargement is iron dependent. *Am J Physiol Cell Physiol*. 2004;287:C1023–C1030. doi: 10.1152/ajpcell.00511.2003
45. Yang L, Nilsson-Payant BE, Han Y, Jaffré F, Zhu J, Wang P, Zhang T, Redmond D, Houghton S, Møller R, et al. Cardiomyocytes recruit monocytes upon SARS-CoV-2 infection by secreting CCL2. *Stem Cell Reports*. 2021;16:2274–2288. doi: 10.1016/j.stemcr.2021.07.012
46. Han Y, Duan X, Yang L, Nilsson-Payant BE, Wang P, Duan F, Tang X, Yaron TM, Zhang T, Uhl S, et al. Identification of SARS-CoV-2 inhibitors using lung and colonic organoids. *Nature*. 2021;589:270–275. doi: 10.1038/s41586-020-2901-9
47. Yang L, Han Y, Nilsson-Payant BE, Gupta V, Wang P, Duan X, Tang X, Zhu J, Zhao Z, Jaffré F, et al. A human pluripotent stem cell-based platform to study SARS-CoV-2 tropism and model virus infection in human cells and organoids. *Cell Stem Cell*. 2020;27:125–136.e7. doi: 10.1016/j.stem.2020.06.015
48. Pharmacists TASoH-S. https://www.drugs.com/monograph/deferoxamine.html. 2016.
49. Nilsson-Payant BE, Uhl S, Grimont A, Doane AS, Cohen P, Patel RS, Higgins CA, Acklin JA, Bram Y, Chandar V, et al. The NF-κB transcriptional footprint is essential for SARS-CoV-2 replication. *J Virol*. 2021;95:e0125721. doi: 10.1128/JVI.01257-21
50. Stuart T, Butler A, Hoffman P, Hafemeister C, Papalexi E, Mauck WM 3rd, Hao Y, Stoeckius M, Smibert P, Satija R. Comprehensive integration of single-cell data. *Cell*. 2019;177:1888–1902.e21. doi: 10.1016/j.cell.2019.05.031
51. de Winter J. Using the Student's t-test with extremely small sample sizes. *Pract Assess Res Eval*. 2013;18:10. doi: 10.7275/e4r6-dj05.